J|A|C|S
ARTICLES

Published on Web 09/23/2010

Structure-Directing Role of Graphene in the Synthesis of Metal−Organic Framework Nanowire

Maryam Jahan,† Qiaoliang Bao,† Jia-Xiang Yang, and Kian Ping Loh*

Department of Chemistry, National University of Singapore, 3 Science Drive 3, Singapore 117543

Received June 10, 2010; E-mail: chmlohkp@nus.edu.sg

Abstract: Graphene can be decorated with functional groups on either side of its basal plane, giving rise to a bifunctional nanoscale building block that can undergo face-to-face assembly. We demonstrate that benzoic acid-functionalized graphene (BFG) can act as a structure-directing template in influencing the crystal growth of metal−organic framework (MOF). BFG is also incorporated into MOF as framework linker. Because of the high density of carboxylic groups on benzoic acid-functionalized graphene, an unusual MOF nanowire that grows in the [220] direction was synthesized. The diameter of the nanowire correlates closely with the lateral dimensions of the BFG. The intercalation of graphene in MOF imparts new electrical properties such as photoelectric transport in the otherwise insulating MOF. The results point to the possibility of using functionalized graphene to synthesize a wide range of structural motifs in MOF with adjustable metrics and properties.

I. Introduction

Graphene, a monolayer of carbon atoms arranged in a 2D honeycomb lattice,[1] has emerged as a promising material for nanoscale electronics.[2] Much of the attention has been directed at the novel electronics properties of this material, but its chemical reactivity is also of great interest and importance. Graphene oxide (GO) derived from the oxidative exfoliation of graphite is solution-dispersible and can act as the precursor to graphene after chemical or thermal reduction. According to the Lerf-Klinowski model of GO,[3] the basal plane of GO is decorated with functional groups such as OH (hydroxyl group) and C−O−C (epoxy group), whereas carboxylic groups are mainly found at the edges. The coexistence of ionic groups and aromatic sp^2 domains allow GO to participate in a wide range of bonding interactions. Because of the solubility and wide-open nature of the GO sheet, it can be functionalized on both sides of the basal planes as well as the edges. Such double-sided decoration not only offers a new class of solution-dispersible polyaromatic platform for performing chemistry but also presents the possibility of a 2D nanoscale building block that can participate in supramolecular assembly to form new hybrids.[4]

Metal organic frameworks (MOFs), especially MOF-5, have attracted intense interests because of potential applications in catalysis,[5] hydrogen storage,[6] and sensors.[7] MOFs can have exceptionally high specific surface area (4 500 m^2g^{-1}) and chemically tunable structure.[8] The 3D grid is assembled from metal clusters interconnected by spatially defined organic linkers, which produce an extended framework with high porosity.[9] It is interesting to consider whether the bifunctionality of GO, in terms of the presence of oxygen functionalities on either side of the sheet, allows it to act as a structural directing agent in molecular assembly. Recently, Petit et al.[10] reported the synthesis of MOF−graphite oxide composite. The suggested model for such a composite is based on the alternation of GO sheets with layers of MOF via linkages between epoxy groups from GO and zinc oxide from the MOF (part a of Scheme 1).[10a] In this case, the intercalation role of GO in MOF structure was

* To whom correspondence should be addressed.
† These authors contributed equally to this work.

(1) (a) Novoselov, A. *Nat. Mater.* **2007**, *6*, 183. (b) Allen, M.; Tung, V.; Kaner, R. *Chem. Rev.* **2010**, *110*, 132. (c) Meyer, J.; Geim, A.; Katsnelson, M.; Novoselov, K.; Booth, T.; Roth, S. *Nature* **2007**, *446*, 60.
(2) (a) Bunch, J. S.; van der Zande, A. M.; Verbridge, S. S.; Frank, I. W.; Tanenbaum, D. M.; Parpia, J. M.; Craighead, H. G.; McEuen, P. L. *Science* **2007**, *315*, 490. (b) Varchon, F.; Feng, R.; Hass, J.; Li, X.; Nguyen, B.; Naud, C.; Mallet, P.; Veuillen, J.; Berger, C.; Conrad, E. *Phys. Rev. Lett.* **2007**, *99*, 126805. (c) Neto, A.; Guinea, F.; Peres, N.; Novoselov, K.; Geim, A. *Rev. Mod. Phys.* **2009**, *81*, 109. (d) Berger, C.; Song, Z.; Li, X.; Wu, X.; Brown, N.; Naud, C.; Mayou, D.; Li, T.; Hass, J.; Marchenkov, A. *Science* **2006**, *312*, 1191. (e) Castro Neto, A.; Guinea, F.; Peres, N.; Novoselov, K.; Geim, A. *Rev. Mod. Phys.* **2009**, *81*, 109. (f) Ang, P. K.; Wang, S.; Bao, Q. L.; Thong, J. T. L.; Loh, K. P. *ACS Nano* **2009**, *3*, 3587. (g) Eda, G.; Fanchini, G.; Chhowalla, M. *Nature Nanotechnol.* **2008**, *3*, 270.
(3) Dreyer, D.; Park, S.; Bielawski, C.; Ruoff, R. *Chem. Soc. Rev.* **2010**, *39*, 228.
(4) Loh, K. P.; Bao, Q. L.; Ang, P. K.; Yang, J. X. *J. Mater. Chem.* **2010**, *20*, 2277.
(5) Tonigold, M.; Lu, Y.; Bredenkötter, B.; Rieger, B.; Bahnmüller, S.; Hitzbleck, J.; Langstein, G.; Volkmer, D. *Angew. Chem., Int. Ed* **2009**, *48*, 7546.
(6) (a) Chen, B.; Ockwig, N.; Millward, A.; Contreras, D.; Yaghi, O. *Angew. Chem., Int. Ed* **2005**, *44*, 4745. (b) Fang, Q.; Zhu, G.; Jin, Z.; Ji, Y.; Ye, J.; Xue, M.; Yang, H.; Wang, Y.; Qiu, S. *Angew. Chem., Int. Ed* **2007**, *46*, 6638. (c) Han, S.; Deng, W.; Goddard, W. *Angew. Chem., Int. Ed* **2007**, *46*, 6289. (d) Li, J.; Cheng, S.; Zhao, Q.; Long, P.; Dong, J. *Int. J. Hydrogen Energy* **2009**, *34*, 1377.
(7) (a) Seo, J.; Whang, D.; Lee, H.; Im Jun, S.; Oh, J.; Jeon, Y.; Kim, K. *Nature* **2000**, *404*, 982. (b) Halder, G.; Kepert, C.; Moubaraki, B.; Murray, K.; Cashion, J. *Science* **2002**, *298*, 1762.
(8) Chae, H.; Siberio-Perez, D.; Kim, J.; Go, Y.; Eddaoudi, M.; Matzger, A.; O'keeffe, M.; Yaghi, O. *Nature* **2004**, *427*, 523.
(9) Hermes, S.; Schroter, M.; Schmid, R.; Khodeir, L.; Muhler, M.; Tissler, A.; Fischer, R.; Fischer, R. *Angew. Chem. Int. Ed* **2005**, *44*, 6237.
(10) (a) Petit, C.; Bandosz, T. J. *Adv. Mater.* **2009**, *21*, 4753. (b) Petit, C.; Bandosz, T. *Adv. Funct. Mater.* **2009**, *20*, 111. (c) Petit, C.; Bandosz, T. J. *J. Mater. Chem.* **2009**, *19*, 6521.

Scheme 1. Schematic of Proposed Bonding between (a) MOF and GO, Monodentate Epoxy Bridges of GO with MOF along the [100] Direction of MOF;[10a] (b) MOF and BFG, Bidentate Carboxylic Bridging of BFG with MOF along the [220] Direction of MOF

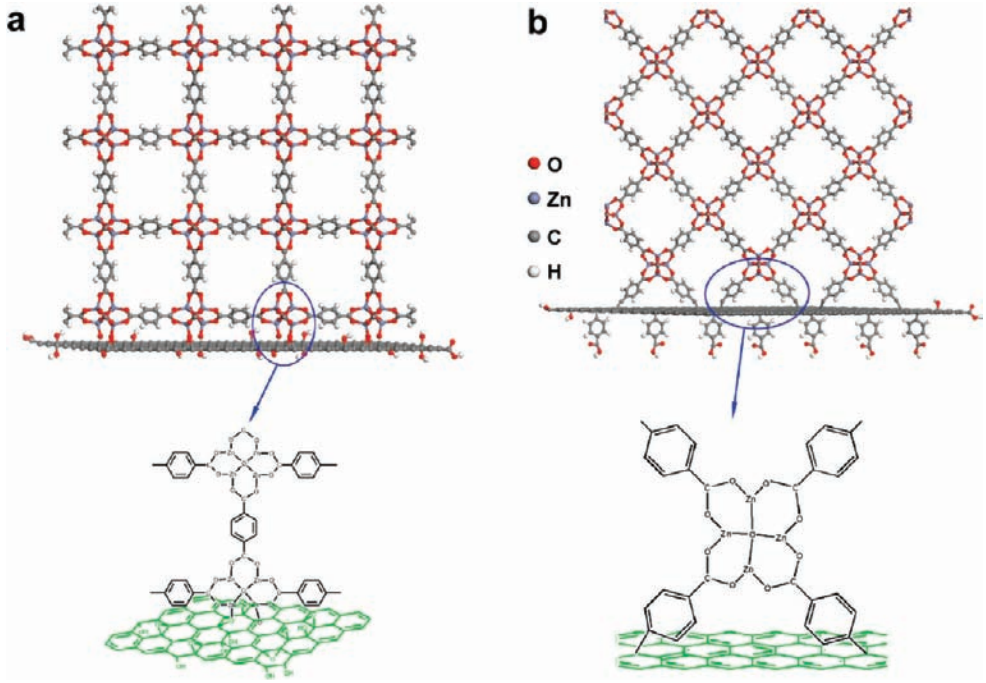

Scheme 2. Schematic Showing Reduction of GO and Functionalization with Benzoic Acid to Form BFG

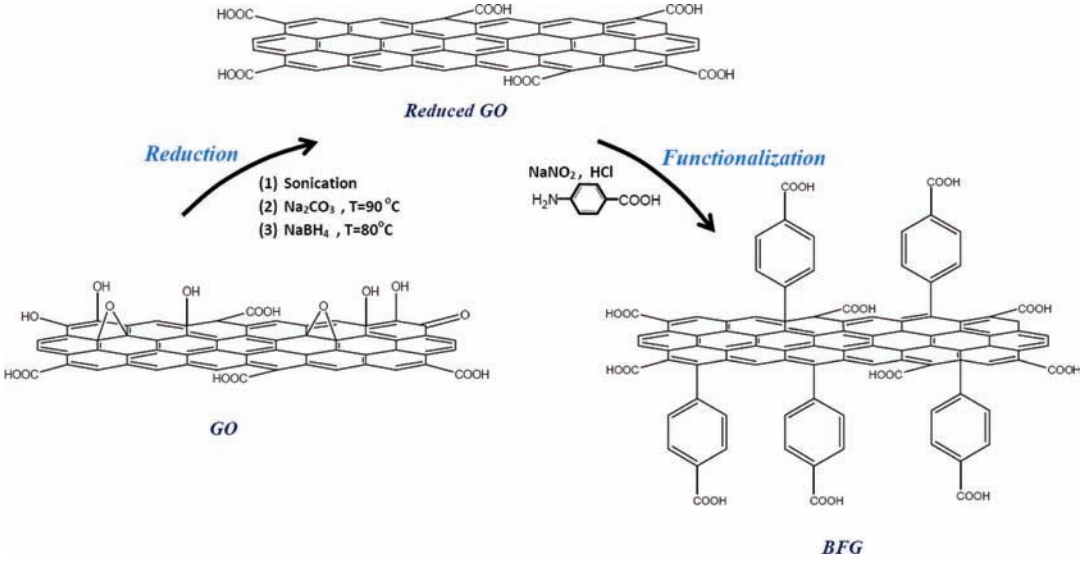

demonstrated, but the potential of GO as a structural directing agent to form a plethora of extended structures uniquely different from classical MOF structures was not manifested. We attribute this to the intrinsic limitation in the metal-chelation abilities of GO, which has little or no carboxylate functionalities on its basal planes.

It is well-known that the choice of metal and organic linker affects the structure and properties of MOF. As an alternative to the monodentate epoxyl linking, the bridging bidentate coordination ability of carboxylate groups favors a higher degree of framework connectivity and stronger metal−ligand bonds (part b of Scheme 1), and this will impart greater structural strength on the MOF architecture. One strategy is to functionalize the basal planes of GO with a high density of carboxylic groups. By controlling the length of the carboxylic linker group and its coverage on the basal plane, a greater degree of tuneability in terms of the structural motif and pore size may be achieved, compared to untreated GO, which has limited chelating agents on the basal planes. To address this, we performed chemical reduction to remove epoxy and hydroxyl groups from the surface of GO. Next, the chemically reduced GO (r-GO) is functionalized with benzoic acid (abbreviated as BFG) using the diazonium grafting method (Scheme 2), and this allows the basal planes to become extended by phenyl carboxylic groups. Finally, by mixing BFG with the precursors used for synthesizing MOF-5, we discovered that BFG can act as both a structure-directing template and framework linker to produce interesting structural motifs in MOF. The electrical properties of MOF were modified with the incorporation of BFG into the network. Here, we report the transport phenomena in

graphene-modified MOF materials, which are rarely reported in literature due to the insulating nature of MOF.

II. Experimental Section

Chemical Reagents. All chemicals purchased were of the purest grade and used as received from Sigma-Aldrich unless otherwise stated.

Graphite Oxide (GO). GO was prepared using a modified Hummers and Offeman's method.[11] In a typical reaction, 0.5 g of graphite, 0.5 g of $NaNO_3$, and 23 mL of H_2SO_4 were stirred in an ice bath for 15 min. Following, 4 g of $KMnO_4$ was slowly added. The solution was transferred to a 35 ± 5 °C water bath and stirred for about 2 h to form a thick green paste. Then, 40 mL of water was added very slowly followed with stirring for 1 h while the temperature was raised to $\sim 90 \pm 5$ °C. Finally, 100 mL of water was added followed by the slow addition of 3 mL of H_2O_2 (30%), turning the color solution from dark brown to pale brown yellowish. The warm solution was then filtered and washed with 100 mL water. The final product was stored under vacuum for drying.

Reduction of GO. In the reduction step, 400 mg GO in a 320 mL water was sonicated for 1 h in order to disperse the GO sheets completely in water. Following, 50 mL (0.047 mol) of 5% sodium carbonate solution was added to adjust the pH to 10 and the solution was then stirred in a round-bottom flask at temperature 90 ± 5 °C for 9 h. This is followed by the addition of 3.2 g sodium borohydride (0.085 mol) in 80 mL water to the GO dispersion, with pH adjusted to 10. The mixture was then kept at 80 °C in an oil bath for 3 h under constant stirring. During the reduction, the dispersion turned from dark brown to black accompanied by outgassing. The resulting product was finally filtered on membrane filter (polyamid) 0.2 μm and washed with water.

Benzoic Acid-Functionalized Graphene (BFG). The phenyl carboxylic diazonium salt was prepared by the following procedures:[12] 960 mg 4-aminobenzoic acid and 280 mg sodium hydroxide (7 mmol) were added to 80 mL water. Following, 526 mg sodium nitrite (7.6 mmol) was added slowly to the solution and the temperature was maintained at 0−5 °C. This solution was added quickly to 6 mL HCl solution (20%, 6.4 M, 19.2 mmol) and stirred for 45 min. The color of solution became pale yellow.

The preparation of BFG was performed by sonicating 300 mg reduced GO dispersed in 1 wt % aqueous sodium dodecylbenzensulfonate (SDBS) surfactant.[13] The diazonium salt solution was added to reduced GO solution in an ice bath under stirring and the mixture was maintained in ice bath at 0−5 °C for around 4 h. Next, the reaction was stirred at room temperature for 4 h. Finally, the resulting solution was filtered using 0.2 μm polyamide membrane and washed several times with water. Because the final product was very soluble in water, HCl solution (pH = 2−3) was added to the solution to protonate the carboxylate groups in order to facilitate the filtration. Then the final product was washed with ethanol, DMF, and acetone.

MOF-5. Large crystals of MOF-5 were synthesized according to published procedures[14] using 1,4-benzenedicarboxylic acid (BDC) and zinc nitrate as the precursors, and dimethylformamide (DMF) as the organic solvent. In a glass reactor equipped with a reflux condenser, 0.2 g of BDC (1.2 mol) and 1.09 g of zinc nitrate hexahydrate (3.6 mol) were dissolved in 30 mL of DMF and heated to 120 °C for 4 h without stirring. Crystallization occurred and the clear solution turned slightly opaque after about 45 min. After reacting for 4 h, the product was allowed to cool to room temperature. The solid was filtered off and immersed in fresh chloroform overnight. The chloroform was changed twice. Finally, the product was dried at 90 °C for three hours under reduced pressure (<0.2 mbar). The resulting crystals were stored in a dedicator.

MOF/BFG Composites. For the synthesis of MOF/BFG composites, varying amounts of BFG (1, 4, and 5 wt %) were added into the dissolved zinc nitrate/BDC mixtures. The resulting suspensions were subsequently stirred and subjected to the same steps as described earlier for the synthesis of MOF-5.[10a]

Instrumentations. Transmission electron microscopy (TEM) analysis was performed with the JEOL 2100 (200 kV) electron microscope. To avoid electron beam-induced damage, low-intensity beam was used for collecting selected area electron diffraction (SAED) patterns. Shorter exposure time was used to capture high resolution TEM images. Scanning electron microscopy (SEM) images were recorded using the JEOL 6701 FESEM at 30 kV. Fourier transform infrared spectroscopy (FTIR) was recorded at room temperature on the Varian 3100 FTIR spectrometer. The samples were ground with KBr and then pressed into disks. Atomic force microscopy (AFM) images were collected in the tapping mode using the SPM D3100 from Veeco and the specimens studied were coated freshly on silica substrates by spin-casting. UV−vis spectroscopic data was collected using the UV-2450 Shimadzu UV−vis Spectrometer with water as the solvent and a path length of 1 cm. N_2 adsorption−desorption isotherms were measured at −196 °C on an automatic volumetric sorption analyzer (Micromeritics, ASAP2020). The Raman spectra were measured with a WITEC CRM200 Raman system. The excitation source is a 532 nm laser (2.33 eV) with a laser power below 0.2 mW on the sample to avoid laser-induced local heating. A 100× objective lens with a numerical aperture (NA) of 0.95 was used in the Raman experiments, and the spot size of a 532 nm laser was estimated to be 500 nm. The spectra resolution of our Raman system is 1 cm^{-1}. Powder X-ray diffraction (XRD) was carried out using a Siemens D5005 X-ray diffractometer with CuKa line (l = 1.54060 A°) as the incident beam which is calibrated by SiO_2. A Gobel mirror was employed as a monochromator. The sample powder was ground and then loaded into a glass holder and leveled with a glass slide before mounting it on the sample chamber. The specimens were scanned at 1.4−50°. The scan step-width was set to 0.005° and the scan rate to 0.005° s^{-1}. XRD data analysis was performed using Reflex module in Materials Studio (Accelrys) software suites (Supporting Information for more details).

To study the electrical properties of single MOF/BFG nanowire, the MOF/BFG ethanolic suspension was spin-coated on SiO_2 substrate. The sample was covered with 600 mesh copper grids as shadow mask, followed by thermal evaporation of 10 nm Cr and 100 nm Au as metal contacts. The electrical and photoelectric transport properties of single MOF/BFG nanowire were measured by a Cascade probe station (Cascade Microtech, USA) connected to an Agilent E5270B 8-Slot Precision Measurement Mainframe (resolution: 0.5 mV and 0.1 fA). To harvest more photocurrent from such MOF/BFG nanowire composite, the nanowire suspension was drop-casted onto interdigital electrodes and the I−V curves were recorded under illumination of solar simulator AMG 1.5 light source (Newport 300W xenon light source, 100 mW/cm^2 intensity).

III. Results and Discussion

Part a of Figure 1 shows UV−vis absorption spectra of GO, r-GO, and BFG in water. The red-shifted $\pi-\pi^*$ absorption band of r-GO at 248 nm compared to the band of GO at 224 nm is consistent with the partial recovery of conjugated network. This red-shift is also apparent for BFG where the scaffold consists of r-GO. BFG shows improved dispersion in DMF and water compared to r-GO. The solution dispersaibility of BFG was examined using UV absorption spectroscopy. A linear relationship between absorbance and concentration (up to 30 mg/L) is

(11) Cote, L.; Kim, F.; Huang, J. *J. Am. Chem. Soc.* **2009**, *131*, 1043.
(12) Si, Y.; Samulski, E. *Nano Lett.* **2008**, *8*, 1679.
(13) Lomeda, J.; Doyle, C.; Kosynkin, D.; Hwang, W.; Tour, J. *J. Am. Chem. Soc.* **2008**, *130*, 16201.
(14) Hafizovic, J.; Bjorgen, M.; Olsbye, U.; Dietzel, P. D. C.; Bordiga, S.; Prestipino, C.; Lamberti, C.; Lillerud, K. P. *J. Am. Chem. Soc.* **2007**, *129*, 3612.

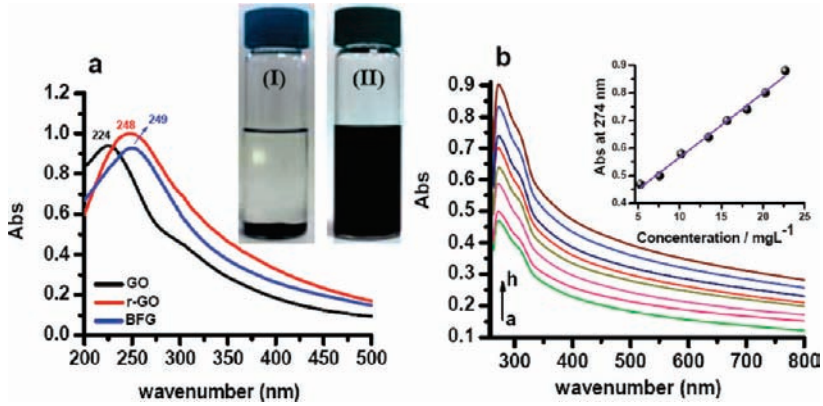

Figure 1. (a) UV−vis absorption spectra of GO (4.3 mg L^{-1}), r-GO (5.8 mg L^{-1}), and BFG (2.5 mg L^{-1}), in water. Insert image: comparison between solubility in DMF of r-GO (I) and BFG (II). (b) Concentration dependence of UV−vis absorption spectra of BFG in DMF (concentration are 5.3, 7.6, 10.2, 13.5, 15.7, 18.1, 20.3, and 23.5 mg L^{-1}, from a−h, respectively). The insert shows the plot of optical density at 274 nm versus concentration. The straight lines are a linear least-squares fit to the data, indicating BFG was dissolved homogeneously in DMF.

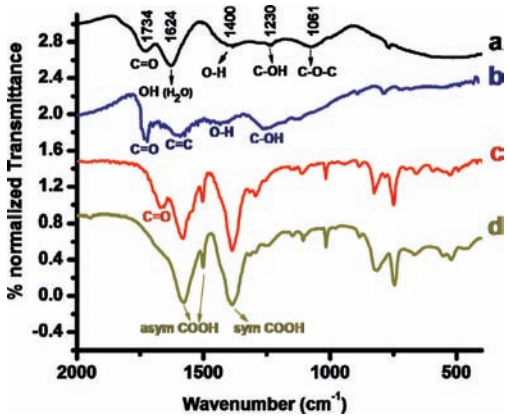

Figure 2. FTIR spectra of (a) GO, (b) BFG, (c) MOF/BFG (5 wt %), and (d) MOF-5.

observed in both DMF and water, which is indicative of good dispersion of BFG because aggregation at high concentration will cause a deviation from linearity in the Beer's plot.

Figure 2 shows the FTIR spectra of GO, BFG, and MOF/BFG. The vibrational peaks of GO are consistent with fingerprint groups such as carboxylic species, hydroxyl species and epoxy species (C═O, 1734 cm^{-1}; OH deformation, 1400 cm^{-1}; the C−OH stretching, 1230 cm^{-1}; C−O−C (epoxy group) stretching, 1061 cm^{-1}; skeletal ring stretch, 1624 cm^{-1}).[15] The FTIR spectrum of BFG (part b of Figure 2) is characterized by a more intense fingerprint *C*═O stretch at 1730 cm^{-1}.[16−18] compared to that of GO, which reflects the higher density of carboxylic groups on the surface. In the spectrum of BFG, we can see that the vibration of the C−O−C (epoxy group) is missing due to the fact that the skeletal framework in BFG is made of reduced GO. A distinctive absorption band which emerges at 1586 cm^{-1} is assigned to the phenyl *C*═C ring stretch of BFG.[19] The FTIR spectrum of MOF-5 (part c of Figure 2) shows bands at 1509 cm^{-1} and 1579 cm^{-1}, which are attributed to the asymmetric stretching of carboxylate group in the BDC moiety, whereas the peak at 1389 cm^{-1} is due to the symmetric stretching of carboxylate group in BDC.[10b] In the region between 1300−700 cm^{-1}, several bands are observed that can be assigned to the out-of-plane vibrations of BDC. The FTIR spectrum of the MOF/BFG (5 wt %) hybrid largely resembles that of MOF-5 (part d of Figure 2). A fingerprint band present at 1675 cm^{-1} is assigned to the *C*═O stretch of carboxylate group located on the surface of BFG. The downshift of the *C*═O stretch from 1730 cm^{-1} to 1675 cm^{-1} in the spectrum of MOF/BFG (5 wt %) is due to the bidentate coordination of the carboxylate group with the zinc clusters in MOF.

To study the structure-composition relationship, different concentration of BFG (1, 4, and 5% by weight) was incorporated along with the chemical precursors of MOF-5 to synthesize graphene/MOF composites. Gradually increasing the content of BFG in the composite will result in increased lattice distortion of MOF, therefore, gradual transformation into new morphologies are expected.

XRD and SEM were used to examine the phase and structure of the synthesized products, as shown in Figure 3. For pure MOF-5, the major diffraction pattern could be assigned to the trigonal crystal class adopting the space group ($R\bar{3}m$ No. 166).[14,20] Weight for weight, it was observed that a small amount of BFG added resulted in more pronounced changes in the structure of MOF compared to pure GO. For example, only 1 wt % BFG was needed to induce similar morphological changes induced by 5 wt % pure GO.[10a] At low incorporation of BFG, thin graphene layers can be seen to act as dividers in the cubic crystal of MOF/BFG (1 wt %), forming a divider-like structure (part b of Figure 3). The important feature of XRD pattern is the splitting of the main diffraction peak (2θ of 9.7°) into two, and the emergence of a new peak at 8.8°, which is correlated with the distortion of lattice structure of MOF-5.[14] Another characteristic is the missing of the key peak at $2\theta = 6.9°$, probably due to disruption of periodicity induced by solvent molecules that fill the mesopores of MOF-5.[21] On the basis of the XRD pattern, MOF/BFG (1 wt %) is assigned to the monoclinic crystal type with lattice parameter $a = 12.023$ Å, *b*

(15) Xu, Y.; Bai, H.; Lu, G.; Li, C.; Shi, G. *J. Am. Chem. Soc.* **2008**, *130*, 5856.
(16) Liu, Y.; Zhou, J.; Zhang, X.; Liu, Z.; Wan, X.; Tian, J.; Wang, T.; Chen, Y. *Carbon* **2009**, *47*, 3113.
(17) Yang, X.; Zhang, X.; Liu, Z.; Ma, Y.; Huang, Y.; Chen, Y. *J. Phys. Chem. C* **2008**, *112*, 17554.
(18) Wang, H.; Hao, Q.; Yang, X.; Lu, L.; Wang, X. *Electrochem. Commun.* **2009**, *11*, 1158.
(19) Sun, X.; Liu, Z.; Welsher, K.; Robinson, J.; Goodwin, A.; Zaric, S.; Dai, H. *Nano Res.* **2008**, *1*, 203.
(20) Eddaoudi, M.; Moler, D.; Li, H.; Reineke, T. M.; O'Keeffe, M.; Yaghi, O. M. *Acc. Chem. Res.* **2001**, *34*, 319–330.
(21) Saha, D. P. D.; Deng, S. G.; Yang, Z. G. *J. Porous Mater.* **2009**, *16*, 141.

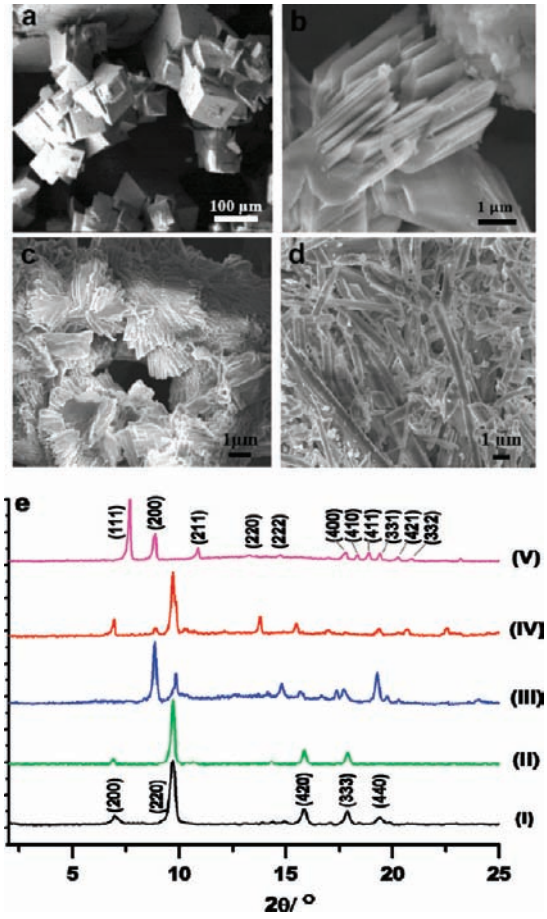

Figure 3. SEM images for (a) MOF-5, (b) MOF/BFG (1 wt %), (c) MOF/BFG (4 wt %), (d) MOF/BFG (5 wt %). (e) XRD patterns of (I) MOF-5, (II) MOF-GO (5 wt %), (III) MOF/BFG (1 wt %), (IV) MOF/BFG (4 wt %), and (V) MOF/BFG (5 wt %).

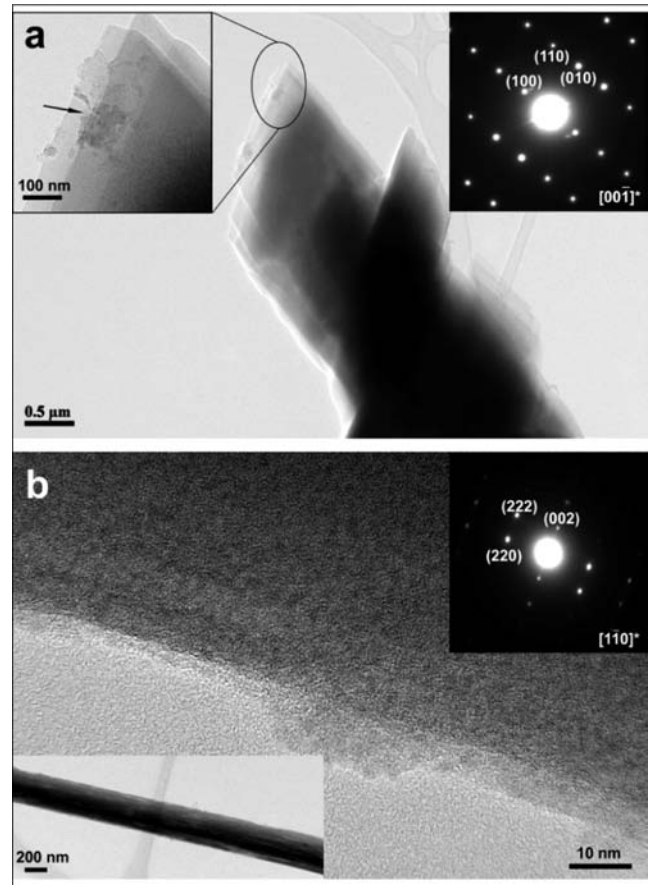

Figure 4. (a) TEM images of MOF/BFG (1 wt %). The upper-left insert shows magnified image and the arrow inside indicates BFG flake. The upper-right insert shows SEAD pattern. (b) HRTEM images of MOF/BFG (5 wt %). The bottom-left insert shows low-magnification image of MOF/BFG nanowire. The upper-right insert shows the SEAD pattern.

$= 5.674$ Å, $c = 18.644$ Å, $\alpha = 90°$, $\beta = 124°$, $\gamma = 90°$, space group: P2/C (No. 13). When the content of BFG is increased to 4 wt %, the composite maintains its monoclinic crystal type with slightly changed lattice parameters ($a = 10.745$ Å, $b = 6.386$ Å, $c = 9.874$ Å, $\alpha = 90°$, $\beta = 112.152°$, $\gamma = 90°$, space group: P2, No. 3). Interestingly, the MOF/BFG composite synthesized with 5 wt % BFG reveals a dramatic transformation into nanowire morphology (part d of Figure 3). The diffraction pattern changes to that of cubic symmetry ($R\bar{3}m$, No. 201) with lattice parameters $a = 19.909$ Å. The reflection originating from (002) plane of BFG becomes more prominent at 5 wt % BFG, which attests to the formation of a hybrid structure (part S3 of the Supporting Information). Another effect caused by the addition of BFG is the broadening of the XRD peaks, due to the formation of smaller sized grains. By measuring the peak-width-at-half-maximum, the grain size of MOF in the composites range from 220 to 260 nm based on the Scherrer equation. To see if this change is unique to BFG, control experiments were performed with GO with its wt % adjusted in a wide range in the composite to see if similar nanowire morphology could be obtained. The results proved that no nanowire morphology could be obtained up to 25 wt % GO. The XRD pattern of MOF/GO (5 wt %) is essentially similar to MOF-5. This proves that the nanowire morphology obtained in MOF/BFG (5 wt %) is unique to the structure-directing ability of BFG. To the best of our knowledge, this represents the first template-free synthesis of MOF nanowires. Previous synthesis of MOF wire bundle by Huang et al.[22] was attained using channel confined growth in anodic alumina template.

TEM was used to investigate the microstructure of the MOF/BFG composites. Part a of Figure 4 examines the structure of MOF/BFG (1 wt %) where faceted MOF sheets can be seen. GO sheets can be seen attached on the MOF-5 sheets, which evidence that intercalation occurred. Part b of Figure 4 shows TEM images and SAED pattern of the MOF/BFG nanowires (MOF/BFG 5 wt %). The nanowire has uniform shape with diameter of ∼300 nm (insert of part b of Figure 4). Energy dispersive X-ray spectroscopy (EDS) analysis reveals the elemental composition to be Zn, O, and C (Figure 5). According to these data the carbon and oxygen content in the MOF/BFG hybrid increases with increasing concentration of BFG. The HRTEM image of the nanowire sidewall clearly resolves dark spots originating from zinc oxide clusters in MOF. The bright spots array in SAED pattern suggests the crystalline nature of the mesopore walls of nanowire. Analysis of the *d*-spacing reveals that the (220) face is stacked along nanowire axis, indicating that nanowire grows along [220] direction. The (220) face of MOF is distinguished by the highest concentration of Zn_4O clusters among all planes. This suggests that the high concentration of carboxylic functional groups on BFG has

(22) Huang, L. M.; Wang, H. T.; Chen, J. X.; Wang, Z. B.; Sun, J. Y.; Zhao, D. Y.; Yan, Y. S. *Microporous Mesoporous Mater.* **2003**, *58*, 105.

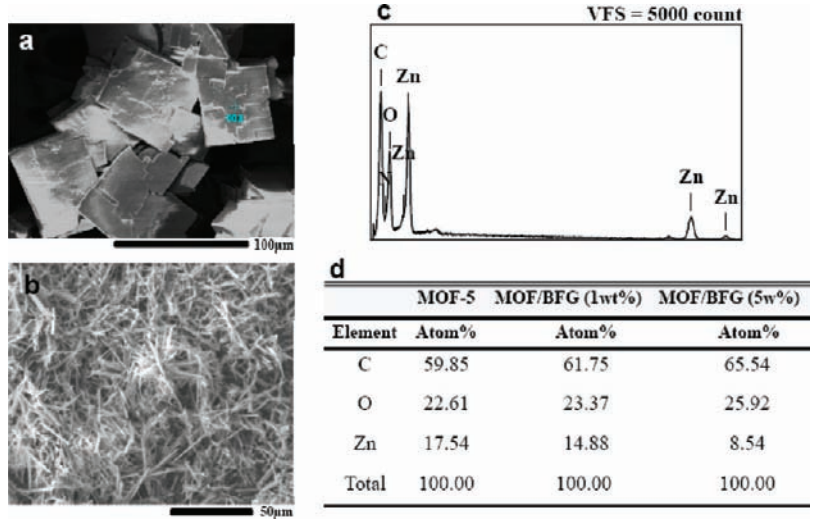

d

	MOF-5	MOF/BFG (1wt%)	MOF/BFG (5w%)
Element	Atom%	Atom%	Atom%
C	59.85	61.75	65.54
O	22.61	23.37	25.92
Zn	17.54	14.88	8.54
Total	100.00	100.00	100.00

Figure 5. (a) SEM image of MOF-5, (b) SEM image of MOF/BFG (5 wt %), (c) EDS spectrum of MOF/BFG (5 wt %) showing the types of elements present in wire structure sample, (d) table compares the atomic percentage of the element consisting in MOF-5, MOF/BFG (1 wt %) and MOF/BFG (5 wt %).

influenced the growth direction in the MOF crystals along the [220] direction due to strong metal−carboxylate binding interactions.

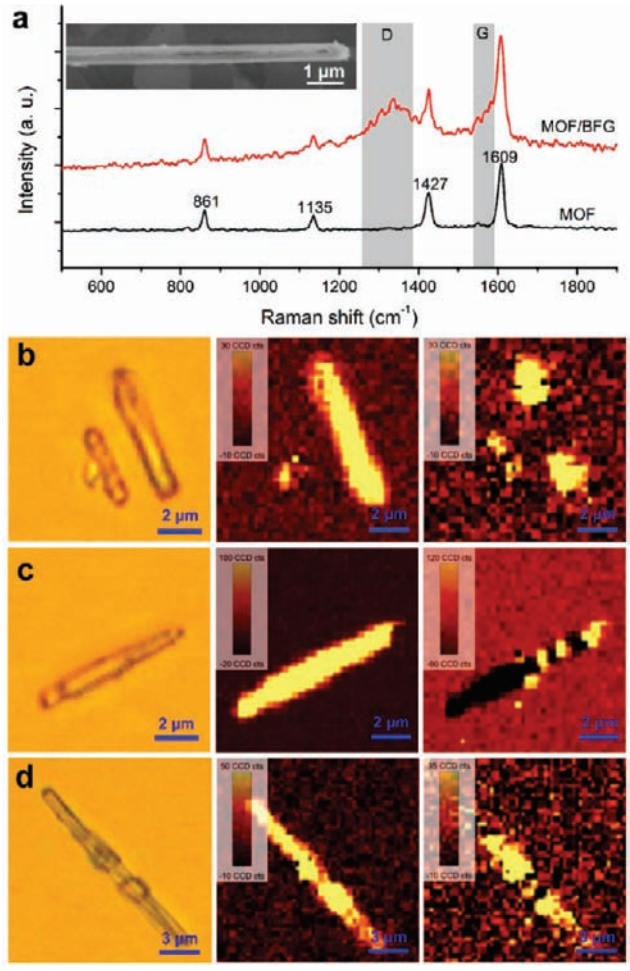

Figure 6. (a) Raman spectra of MOF and MOF/BFG (5 wt %). Insert shows SEM image of an individual MOF/BFG nanowire. (b−d) Raman mapping of MOF/BFG nanowires. Left: optical image. Medium: Raman maps integrated by Raman band at 1609 cm^{-1}. Right: Raman maps integrated by D band of graphene.

Micro-Raman spectroscopy was performed to verify the existence of BFG in the nanowires, as shown in Figure 6. Four main vibration bands can be resolved in the Raman spectra of pristine MOF-5 (part a of Figure 6), and three of these (1609, 1427, and 1135 cm^{-1}) are associated with the in-plane and out-of-phase stretching modes of the C−H groups in benzene ring.[23] The Raman band at 861 cm^{-1} is due to the out-of-plane deformation modes of the C−H groups. For MOF/BFG, we did not observe obvious peak shifts of the MOF bands in Raman except for the appearance of bands associated with graphene. The Raman G band of graphene at around 1590 cm^{-1} slightly overlaps with the Raman band at 1609 cm^{-1} of MOF; nevertheless, the broad D band of graphene at around 1350 cm^{-1} can be unambiguously observed. Therefore, D band can be used as a signature to locate graphene in BFG−MOF nanowires, as shown by the Raman mapping images in parts b−d of Figure 6. On the basis of careful Raman analysis, we found that graphene flakes in BFG−MOF nanowires are distributed in three

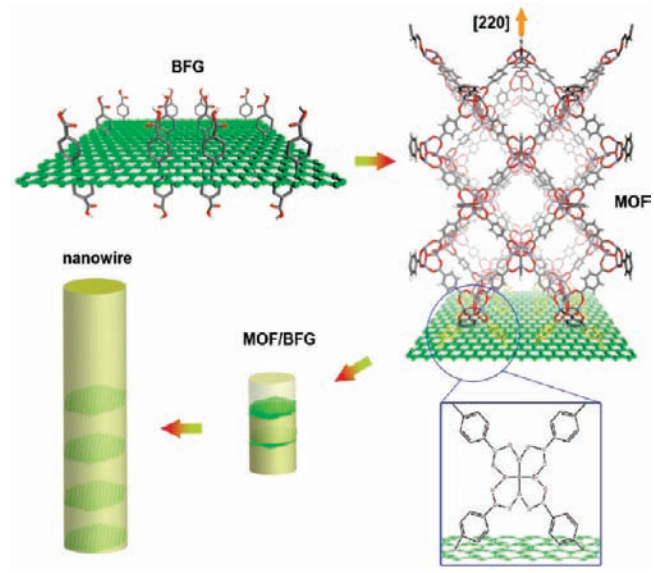

Figure 7. Schematic of proposed bonding between functionalized graphene and MOF via −COOH groups along [220] direction and the assembly into nanowire structure.

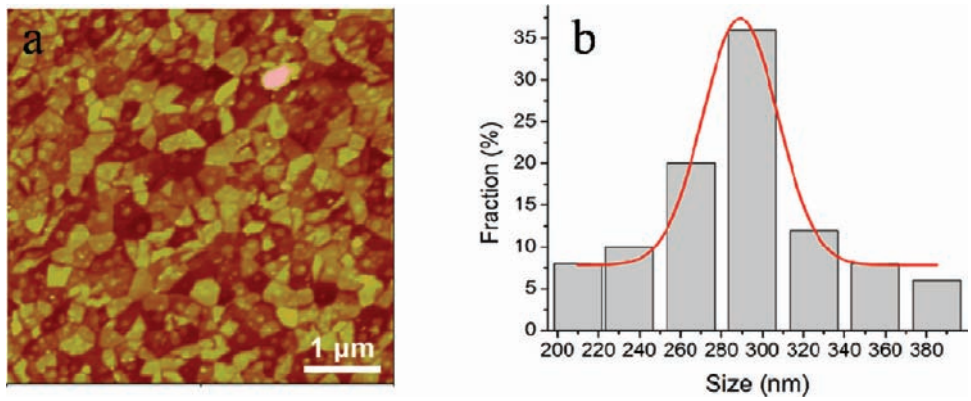

Figure 8. (a) Typical AFM topology of BFG on Si substrate. (b) Histogram of the size distribution of BFG flakes with a Gaussian fit centered at 290 nm.

ways, that is, predominantly at the tips (part b of Figure 6), periodically distributed along nanowire (part c of Figure 6) and distributed along the whole nanowire (part d of Figure 6). The fact that most MOF/BFG has graphene at the tips suggests that it might follow a tip-growth mechanism in which BFG acts as the template for the nucleation of MOF. The intercalated graphene inside the nanowire (part c of Figure 6) indicates that BFG acts as a linker in the MOF framework. SEM analysis (insert of part a of Figure 6) of the exterior of individual MOF/BFG nanowire reveals that the surface of the nanowire is smooth and no adsorbed sheets can be seen. This suggests that most of BFG sheets are intercalated into MOF.

On the basis of the structural analysis, a growth mechanism of MOF/BFG nanowires is proposed, as shown in Figure 7. Because the main functional groups on the basal planes of BFG are phenyl carboxylic groups, it can be conceived that that nucleation begins with the anchoring of zinc oxide cluster on the BFG planes via metal−carboxylate bonds. Similar type of template-directed interaction was reported by Camilla and coworkers[24] who investigated the oriented growth of MOF crystals on mercaptohexdecanoic acid self-assembled monolayer on an Au (111) surface.

It is worthwhile asking why the growth of the MOF/BFG nanowire only occurred at high concentration of BFG (5 wt %). This is in fact consistent with a kinetically controlled template-directed growth model, where the BFG acts as the nucleation template. At low concentration of BFG, the rate of growth of MOF crystals is controlled largely by MOF precursors such as 1,4-benzoic acid and zinc ions and the crystal morphology is mainly associated with the classical MOF-5 crystal shape (i.e., cubes). The addition of BFG merely introduces intercalating sheets into the MOF-5 with increasing disruption of the lattice periodicity. This situation changes dramatically at high concentration of BFG, the presence of a high density of carboxylic groups on our BFG sheets will compete for the Zn ions and shifts the kinetic equilibrium, which ultimately influences the growth direction of the crystal. Acid base titrations have been used to assay the amount of carboxylic groups in GO and BFG.[25] (part S1 in the Supporting Information). GO contains 0.0061 mmol of COOH groups per milligram of GO, whereas BFG contains 0.0178 mmol of COOH groups per mg/BFG. The 3-fold increase of COOH groups in BFG compared to GO provides evidence of the successful functionalization of the basal planes of reduced GO with benzoic acids. As discussed earlier, the BFG template selects the (220) plane of MOF which has the highest density of ZnO clusters, this results in the template-directed growth along the (220) direction as evidenced by TEM analysis of the MOF nanowire. The lack of sufficient coverage of carboxylic functional groups on untreated GO do not avail itself to this added channel of reaction, hence no nanowires can be formed for all concentrations of GO tested. Another implicit question is whether there exists a correlation between the size of the BFG and the diameter of the nanowire, since our Raman analysis reveals that BFG not only acts as a nucleation template but also get intercalated in the wire. According to size counting by AFM (Figure 8), the average diameter of the graphene sheets we used is in the range of 300 ± 30 nm, which coincides with the diameter of the MOF nanowires synthesized as well as the average grain size estimated from XRD peak width. This attests to the validity of the template-directed growth model.

The sorption properties of the MOF/BFG were investigated by recording the N_2 sorption isotherms (Figure 9). The isotherm reveals that the MOF/BFG samples exhibit typical

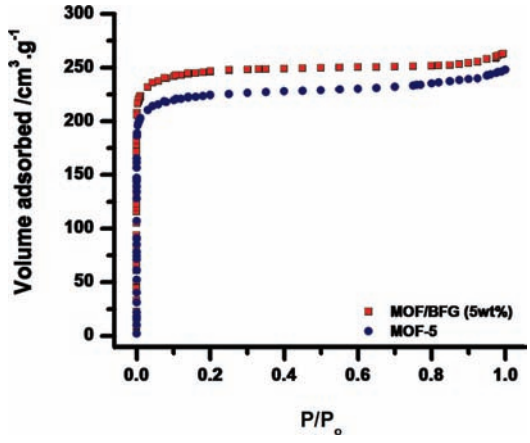

Figure 9. Nitrogen gas sorption isotherm at 77 K for MOF-5 and MOF/BFG nanowire. P/P_0 is the ratio of gas pressure (P) to saturation pressure (P_0) with P_0 = 746 Torr.

Table 1. Adsorption Properties of MOF-5 and MOF/BFG (5 wt %)

sample	BET surface area (m^2/g)	micropore area (m^2/g)	external surface area (m^2/g)	micropore volume (cm^3/g)	total area in pore (m^2/g)
MOF-5	800.83	704.73	96.09	0.326	781.38
nanowire	809.76	711.68	101.28	0.329	789.62

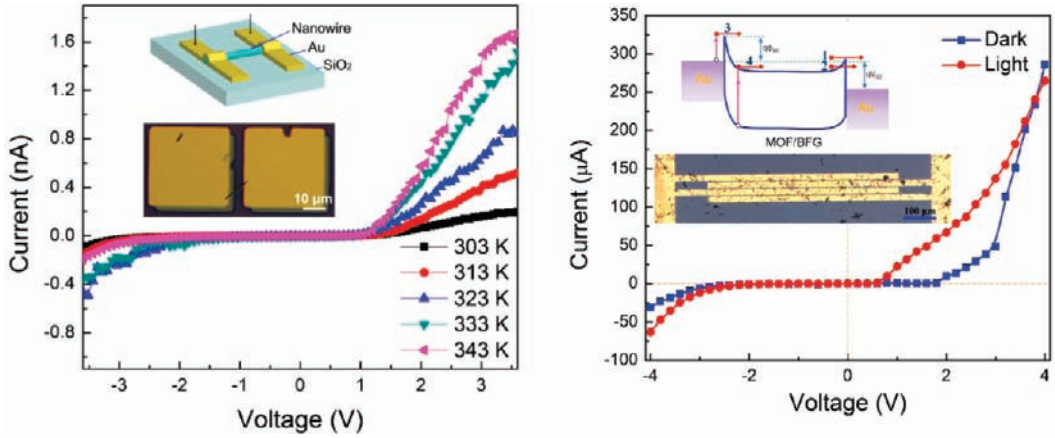

Figure 10. (a) $I-V$ curve of single MOF/BFG nanowire measured at different temperature. Insert shows schematic (upper) and optical image (lower) of the two-electrode device. (b) $I-V$ curve and photocurrent measured on an interdigited device using MOF/BFG nanowires adsorbed with dye molecules. Lower insert shows the optical image of the device. Upper insert illustrates the schematic energy band diagram of the device. 1. Thermionic emission; 2. Tunneling; 3. Excitation over the barrier; 4. Band-to-band excitation.

type I sorption behavior without hysteresis.[26] As derived from the N_2 adsorption data, the Brunauer−Emmett−Teller surface area of MOF/BFG (5 wt %) is higher than MOF-5, which indicates that intercalated graphene increases the surface area in porous MOF-5. However, the difference between nitrogen adsorption of nanowire and MOF-5 is not so significant.

BET nitrogen adsorption isotherms were recorded to study the effect of BFG in increasing the surface area of MOF-5. The BET surface area and microporosity of our synthesized MOF-5 is similar to that reported by Petit et al.[10a] From these isotherms, the parameters of the porous structures were mentioned in Table 1. The results show that the surface area and microporosity of MOF/BFG is only marginally improved over that of MOF-5, due perhaps to the low wt % (5%) of graphene used in the experiments. Although the BET surface area and microporosity of our synthesized MOF-5 is close to that reported by Huang et al.,[22] it should be noted that the surface area reported of the MOF-5 here is much smaller than 3500 $m^2\ g^{-1}$, the highest value reported.[27] This is due to the fact the preparation conditions for our MOF-5 had not been optimized.

The electrical properties of MOF-5 were very rarely studied due to the insulating nature of the zinc−oxygen tetrahedra and phenylene bridges. When the MOF/BFG wire is placed across source and drain metal electrodes, the system can be considered as a metal−dielectric−metal system. The presence of graphene may change the dielectric breakdown strength of the material, or allow Frenkel-Poole type conduction via high density of charge traps. The electrical property of single MOF/BFG nanowire was first studied by fabricating two-probe electrical devices, as shown in part a of Figure 10. To form good contact and reduce resistance, gold electrodes were deposited on top of nanowire by using squared copper grids as shadow mask. The schematic and optical images of the device are illustrated by the inserts of part a of Figure 10. The $I-V$ curve obtained from single MOF/BFG nanowire shows almost no conduction at low field, which attests to the generally insulating nature of the MOF−BFG system. In MOF/BFG, the intercalating G is perpendicular to the field transport direction and separated spatially by MOF, so a low resistance percolation pathway is absent. The rectification behavior can be attributed to Schottky contact between MOF/BFG and gold contact. The current increases sharply at voltage >4 V, due to thermionic emission. It is interesting that when the device was illuminated by white light, the current can be enhanced significantly, we attribute this to photoinduced charge transfer.

One advantage of the BFG/MOF hybrid is its open framework structure that allows the loading of dyes onto the graphene plane. For this purpose, the MOF/BFG nanowire was immersed in ethanol solution of dichlorotris (1,10phenanthroline) ruthenium(II) hydrate to soak up the dye. Following, the nanowires were drop-casted onto interdigited electrodes, as shown in part b of Figure 10 and in the inserts. The threshold for current rise now starts at a lower voltage of <1.8 V, its magnitude has increased and the current appears to be linear for some voltages before rising exponentially. This proves that the open framework structure of the BFG/MOF wire allows the efficient loading of dye as well as its photoexcitation and charge injection to produce significant enhancement in the photocurrent. A schematic energy band diagram was proposed to explain these electrical behaviors, as illustrated by the insert of Figure 10b. Without illumination, the major transport processes are thermionic emission and tunneling. Under illumination, excitation over the barrier and band-to-band excitation may occur and contribute to the photocurrent. The ability to modify the MOF/BFG framework with organic dyes to produce a strong photoresponse suggests that photocatalysis may be feasible for such hybrid structures.

IV. Conclusions

In conclusion, we show that benzoic acid-functionalized graphene (BFG), in addition to acting as an integral component of the MOF framework, can also act as a structure-directing agent in MOF synthesis. Compared to untreated GO, BFG affects the crystallization of MOF in a more pronounced way. At 5% weight composition of BFG, an unusual MOF/BFG

(23) Bordiga, S.; Lamberti, C.; Ricchiardi, G.; Regli, L.; Bonino, F.; Damin, A.; Lillerud, K. P.; Bjorgen, M.; Zecchina, A. *Chem. Commun.* **2004**, *20*, 2300.
(24) Scherb, C.; Schodel, A.; Bein, T. *Angew. Chem., Int. Ed* **2008**, *47*, 5777.
(25) Xiaoying, Y.; Xiaoyan, Z.; Yanfeng, M.; Yi, H.; Yinsong, W.; Yongsheng, C. *J. Mater. Chem.* **2009**, *19*, 2710.
(26) Son, W.; Kim, J.; Ahn, W. *Chem. Commn.* **2008**, *47*, 6336.
(27) Kaye, S. S.; Dailly, A.; Yaghi, O. M.; Long, J. R. *J. Am. Chem. Soc.* **2007**, *129*, 14176.

nanowire was synthesized, which could be attributed to the template-directed nucleation effect of BFG. The results point to the possibility of using functionalized graphene to synthesize a wide range of structural motifs in MOF with adjustable metrics and properties. The conductivity and high specific surface area of graphene can impart new properties on MOF. The versatile functionalization of graphene with organic molecules allows it to act as nanoscale building blocks in designing MOF hybrids with potential applications in organocatalysis and sensors.

Acknowledgment. K.P. Loh acknowledges NRF-CRP grant "Graphene Related Materials and Devices." R-143-00-360-281.

Supporting Information Available: This material is available free of charge via the Internet at http://pubs.acs.org.

JA105089W